PERGAMON

International Journal of Heat and Mass Transfer 45 (2002) 3173–3180

International Journal of HEAT and MASS TRANSFER

www.elsevier.com/locate/ijhmt

Analytic solution for the non-linear drying problem

L. Pel [a,*], K.A. Landman [b], E.F. Kaasschieter [c]

[a] Department of Applied Physics, Eindhoven University of Technology, P.O. Box 513, 5600 MB Eindhoven, Netherlands
[b] Department of Mathematics and Statistics, University of Melbourne, Victoria 3010, Australia
[c] Department of Mathematics and Computer Science, Eindhoven University of Technology, P.O. Box 513, 5600 MB Eindhoven, Netherlands

Received 23 May 2001; received in revised form 7 November 2001

Abstract

Recently, Landman, Pel and Kaasschieter proposed an analytic solution for a non-linear drying problem using a quasi-steady state solution. This analytic model for drying is explained here. An important consequence of this model is that the drying front has a constant speed when it is entering the material. This is also observed in experiments. On the basis of this constant drying front speed comparisons are made between the analytic model and numerical simulations. Finally comparisons are made between measured moisture profiles during drying and the analytic model. © 2002 Elsevier Science Ltd. All rights reserved.

Keywords: Drying; Modelling; Porous media

1. Introduction

Drying of porous media is a current topic of research in many areas, e.g., chemical engineering, civil engineering and soil science. A thorough understanding of drying will have many technical and economic consequences. In engineering applications one prefers a simple, but adequate description, which simulates the drying of a material correctly. It is usual for the moisture transport to be described by a non-linear diffusion model (see, e.g., [1–17])

$$\frac{\partial\theta}{\partial t} = \frac{\partial}{\partial x}\left(D(\theta)\frac{\partial\theta}{\partial x}\right). \tag{1}$$

In this equation θ is the moisture content and $D(\theta)$ is the moisture diffusivity. In this 'lumped' model all mechanisms for moisture transport, i.e., liquid flow and vapour diffusion, are combined into a single moisture diffusivity, which is dependent on the actual moisture content. Whitaker [2] and Bear and Bachmat [3] provide a more fundamental basis for this diffusion model using volume-averaging techniques.

For the one-dimensional drying problem considered here the boundary condition at the left drying surface is given by

$$D(\theta)\frac{\partial\theta}{\partial x} = \beta(h_{\mathrm{m}}(\theta) - h_{\mathrm{a}}), \tag{2}$$

where β is the mass transfer coefficient, h_{a} is the relative humidity of the exterior air and $h_{\mathrm{m}}(\theta)$ is the relative humidity of the material at the surface which is determined by the desorption isotherm. At the vapour-tight right-hand side there is a no-flux condition.

In general two stages can be identified during the drying process. Initially the drying is determined by the external conditions, i.e., the moisture transport in the material is faster than the mass transfer out of the material by the air flow. As a result, the moisture profiles in the material will be rather flat and uniform. However, as soon as the air-blown surface becomes dry a drying front will enter the material. Now it is the internal moisture transport that limits the drying rate of the material. Both the drying rate and the heat extracted from the sample are strongly decreased. In general from this time onwards the drying experiment can be considered as isothermal (see e.g., [4,5]). During this second stage the

* Corresponding author. Tel.: +31-40-2473406/+31-40-2474248; fax: +31-40-2432598.
E-mail address: l.pel@tue.nl (L. Pel).
http://www.phys.tue.nl/nfcmr/cmrmain.html

0017-9310/02/$ - see front matter
PII: S0017-9310(02)00025-X

Nomenclature

A_1	constant (m^2 s^{-1})	U	constant (dimensionless)
A_2	constant (m^2 s^{-1})	x	position (m)
b_1	constant (dimensionless)	α	function (dimensionless)
b_2	constant (dimensionless)	β	mass transfer coefficient (m s^{-1})
D	moisture diffusivity (m^2 s^{-1})	Δ	moisture diffusivity (dimensionless)
g	function (dimensionless)	θ	moisture content (m^3 m^{-3})
h_a	relative humidity of the air (dimensionless)	θ_m	moisture content at minimum of the moisture diffusivity (m^3 m^{-3})
h_m	relative humidity of the material (dimensionless)	θ_∞	moisture content at which the relative humidity of the material matches h_a (m^3 m^{-3})
L	sample length (m)	ξ	position (dimensionless)
s	position of drying front (dimensionless)	τ	time (dimensionless)
S	position of drying front (m)		
t	time (s)		

moisture profiles, which exhibit a moving drying front, are determined by the material properties such as moisture diffusivity.

This moisture diffusivity $D(\theta)$ must be determined experimentally for the porous material of interest. By measuring the transient moisture profiles during drying, the diffusion coefficient can be determined directly (see e.g., [4,5]). The resulting moisture diffusivity has a deep minimum for many building materials, as shown for fired-clay brick [4–8], clay [9,10], sand–lime brick [5,6], gypsum [5,11], cellular concrete [7,12], mortar [8] and soil [13,14]. In Fig. 1 the general form of the moisture diffusivity is indicated by the dashed line.

From the shape of the moisture diffusivity curve in Fig. 1, two regimes can be identified that relate to certain ranges of the moisture content. At high moisture contents the moisture transport is dominated by liquid transport. With decreasing moisture content the large pores will be drained and will therefore no longer contribute to liquid transport. Subsequently the moisture diffusivity will decrease. Below a so-called critical moisture content, the water in the sample no longer forms a continuous phase or the transport between remaining water clusters has become very low. Hence the moisture has to be transported by vapour and this transport will therefore be governed by the vapour pressure. For low moisture contents the moisture diffusivity begins to increase again. The minimum in the moisture diffusivity therefore indicates the transition from moisture transport dominated by liquid transport to moisture transport dominated by vapour transport. This transition from liquid to vapour transport corresponds to the drying front in the moisture profiles.

Using such measured moisture diffusivity relations, the drying process can be simulated under various conditions and geometries. Until now, numerical simulations have been the only way to solve the non-linear diffusion equation. However, numerical simulations provide no basic understanding of the drying process. Recently Landman et al. [18] proposed an analytic solution based on quasi-steady states which broadens our understanding of the drying process. It is beyond the scope of this article to go into the full details of the mathematical derivation of the solution. In this paper the discussion will be limited to the second drying stage during which the drying is internally limited and the moisture profiles exhibit a front. Here the analytic model will be compared with numerical simulations. Further-

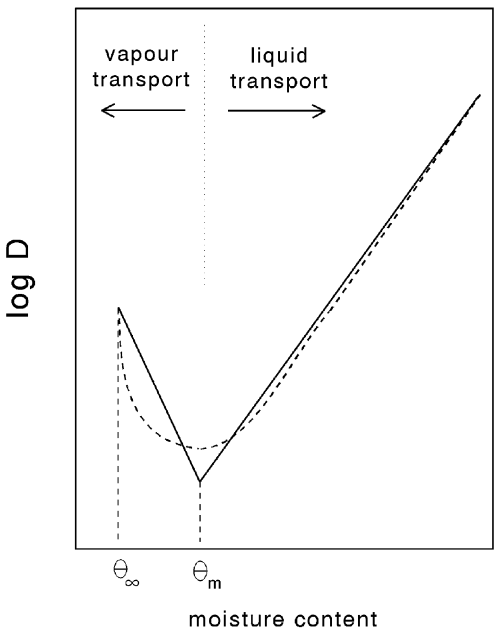

Fig. 1. The general form of the moisture diffusivity and the approximation of this diffusivity as used in the analytic model.

more, a comparison is made between analytic solutions and the measured moisture profiles during drying of fired clay brick, sand–lime brick and gypsum. Finally, also a comparison is made between the moisture diffusivity determined from the measured moisture profiles and those determined by fitting the analytic model to the measured moisture profiles.

2. The analytic solution

The drying problem can be restated in the following dimensionless form:

$$\frac{\partial\theta}{\partial\tau}=\frac{\partial}{\partial\xi}\left(\Delta(\theta)\frac{\partial\theta}{\partial\xi}\right), \tag{3}$$

where the dimensionless spatial position is given in terms of L, the length of the sample

$$\xi=\frac{x}{L}. \tag{4}$$

For our materials, there is a clear and deep minimum in the moisture diffusivity, occurring at a moisture content denoted by θ_m. Here we have chosen to scale the moisture diffusivity relative to this minimum in the moisture diffusivity as

$$\Delta(\theta)=\frac{D(\theta)}{D(\theta_m)} \tag{5}$$

and to scale the time variable by:

$$\tau=\frac{D(\theta_m)}{L^2}t. \tag{6}$$

In the second drying stage when the drying is internally limited, the boundary conditions are well approximated by

$$\theta(0,\tau)=\theta_\infty, \tag{7}$$

$$\frac{\partial\theta}{\partial\xi}(1,\tau)=0, \tag{8}$$

where the boundary moisture content θ_∞ is given by

$$h_m(\theta_\infty)=h_a. \tag{9}$$

In order to obtain a fully analytic solution, the moisture diffusivity will be approximated by:

$$\begin{aligned} &D(\theta)=A_1e^{b_1\theta}, \quad \theta\geqslant\theta_m,\\ &D(\theta)=A_2e^{-b_2\theta}, \quad \theta\leqslant\theta_m, \end{aligned} \tag{10}$$

as illustrated by the straight lines in Fig. 1. Hence the material moisture diffusivity is characterized in the liquid moisture transport phase by the parameters A_1 and b_1, and in the vapour transport phase by the parameters A_2 and b_2. Alternatively one can also characterize the diffusivity by $D(\theta_m)$, θ_m, b_1, and b_2. Hence the scaled moisture diffusivity is given by

$$\begin{aligned} &\Delta(\theta)=e^{b_1(\theta-\theta_m)}, \quad \theta\geqslant\theta_m,\\ &\Delta(\theta)=e^{-b_2(\theta-\theta_m)}, \quad \theta\leqslant\theta_m. \end{aligned} \tag{11}$$

It should be noted that $D(\theta_m)$ and the actual minimal moisture diffusivity may be different. Using a quasi-steady state solution Landman et al. [18] show that the moisture profiles are given by

$$\theta(\xi,\tau)=\theta_m+\frac{1}{b_1}\left[\ln\left(1-b_1U+\frac{\xi}{g(\tau)}\right)-\frac{\xi-b_1Ug(\tau)}{1+(1-b_1U)g(\tau)}\right], \quad \theta\geqslant\theta_m, \tag{12}$$

$$\theta(\xi,\tau)=\theta_m-\frac{1}{b_2}\ln\left(1+b_2U-\frac{b_2}{b_1}\frac{\xi}{g(\tau)}\right), \quad \theta\leqslant\theta_m. \tag{13}$$

Here Eq. (12) describes the liquid dominated part of the moisture profiles, whereas Eq. (13) describes the vapour dominated part. The parameter U is given by

$$U=\frac{1}{b_2}\left(e^{b_2(\theta_m-\theta_\infty)}-1\right) \tag{14}$$

and the function $g(\tau)$ is defined in terms of the front position.

The moisture content θ_m corresponding to the minimum in the moisture diffusivity indicates the position of the front. We call this position $s(\tau)$, so that $\theta(s(\tau),\tau)=\theta_m$. In the quasi-steady state solution this position is given in terms of $g(\tau)$ as

$$s(\tau)=b_1Ug(\tau). \tag{15}$$

In Fig. 2, typical quasi-steady state moisture profiles as given by the analytic approximations Eqs. (12) and (13) are illustrated for increasing values of $g(\tau)$. As can be seen these profiles clearly show a drying front entering the material, and the moisture content corresponding to the minimum in the moisture diffusivity indicates the position of the front.

In order to give the solution explicitly in dimensionless time τ it can be shown that the function $g(\tau)$ can be approximated by a linear function as

$$g(\tau)=\alpha\left(b_1U,\frac{b_1}{b_2}\right)\tau. \tag{16}$$

The complete expression for α is given in the Appendix A. Since the position of the drying front is linear with time, the drying front has a constant speed as it is entering the material, i.e.

$$\frac{ds(\tau)}{d\tau}=b_1U\alpha\left(b_1U,\frac{b_1}{b_2}\right). \tag{17}$$

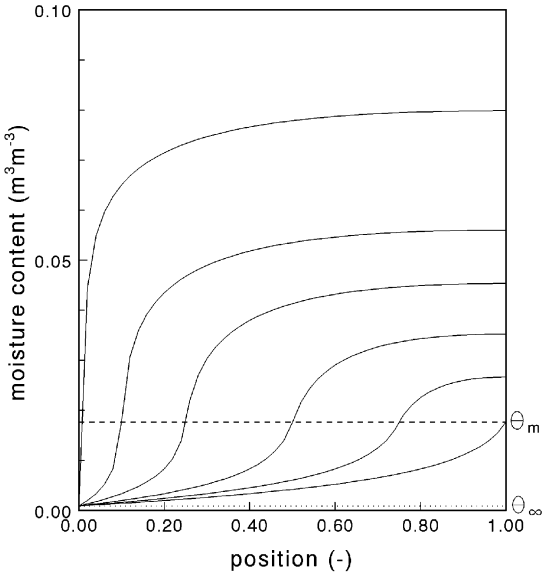

Fig. 2. The moisture profiles during drying for various values of the front position $s(\tau)$, namely for $s(\tau)$ equal to 0.01, 0.1, 0.25, 0.5, 0.75 and 1.0. These profiles are given using $A_1 = 0.003$, $b_1 = 100$, $A_2 = 0.006$ and $b_2 = 200$.

This can be rewritten back to

$$\frac{dS(t)}{dt} = b_1 U \frac{D(\theta_m)}{L} \alpha\left(b_1 U, \frac{b_1}{b_2}\right), \tag{18}$$

where S is the position of the front in real coordinates. Hence as can be seen from Eq. (18) the speed of the front is not only determined by the vapour transport, i.e., the parameters U and b_2 but is also determined by the liquid moisture transport, i.e, the parameter b_1.

In various experiments [5,6,10], the moisture profiles were measured as a function of time. For these, the time evolution of the drying front position can be determined as illustrated in Fig. 3. As clearly illustrated in all cases there is an approximately linear relation between the position of front and the time. Hence the drying front has a constant speed as predicted from the analytic solution (Eq. (17)). This linear relationship was also found by van Brakel [19]. He was, however, unable to explain this on the basis of a model.

3. Comparisons between the analytic model and numerical simulations

The constant speed of the drying front gives a good basis for benchmarking the analytic solution with a numerical simulation. Moisture profiles during drying were computed using standard procedures from the NAG-library for various combinations of b_1, b_2 and θ_m. From these simulated profiles the speed of the drying front was calculated from a linear fit of the position of the front between $0.1 < \xi < 0.8$. In Fig. 4 the numerically determined speed from a simulation is plotted against the calculated speed of the drying front from the analytic

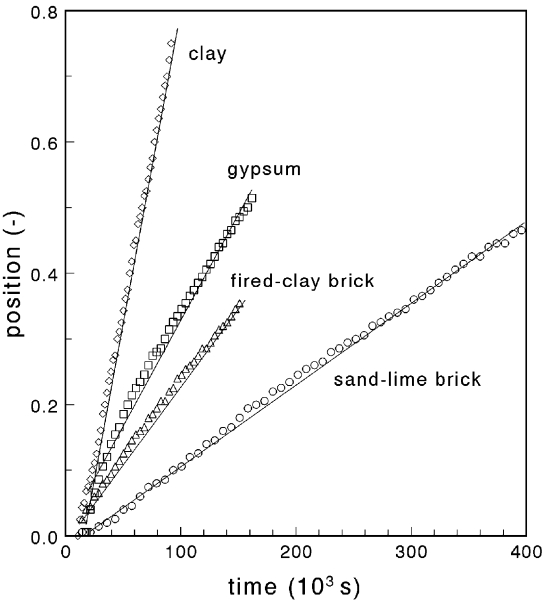

Fig. 3. The dimensionless position of the drying front for various drying experiments: clay [8], gypsum [4,9], fired-clay brick [4,5] and sand–lime brick [5].

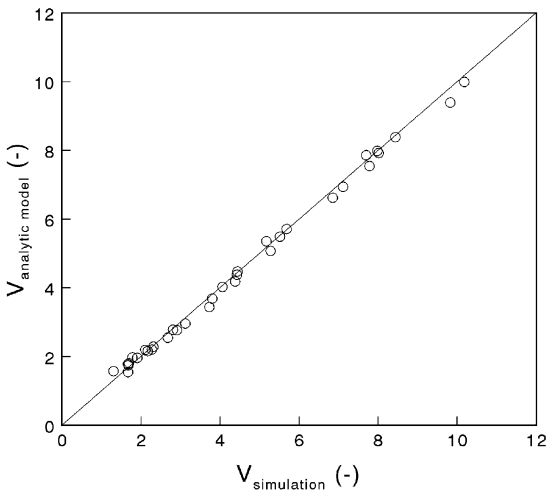

Fig. 4. The analytic speed of the drying front plotted against the numerically calculated speed of the drying front for various combinations of b_1, b_2 and θ_m. Each of the numerical speeds represents the value determined from a numerical simulation of the drying.

model. This figure clearly illustrates that an excellent agreement (within 2%) between the two speeds is found. This indicates the accuracy of the analytic solution to the non-linear diffusion equation describing the second stage of the drying process.

4. Examples of drying behaviour and comparison with the analytic model predictions

Finally a comparison was made between the moisture profiles measured during the drying process and

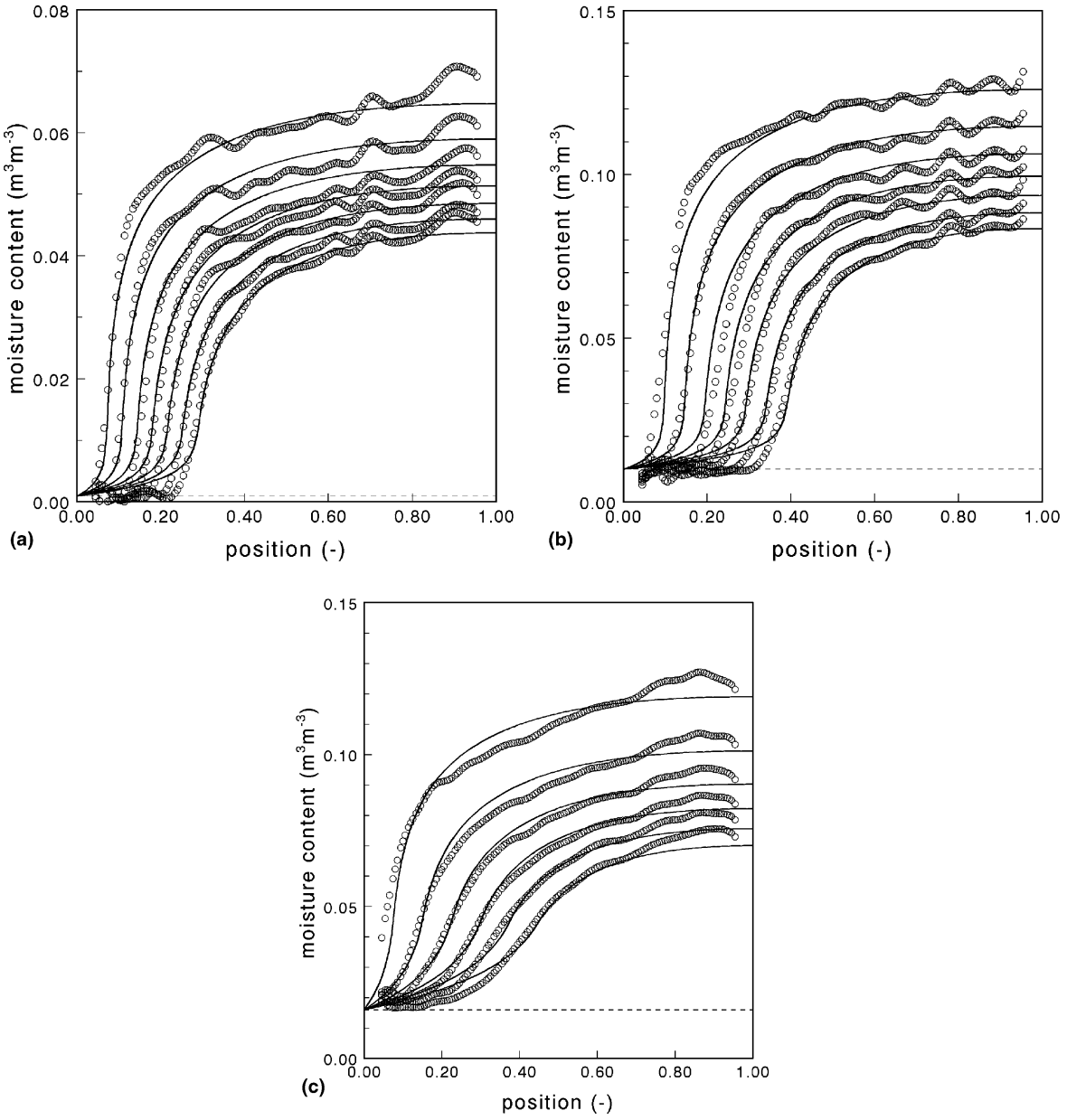

Fig. 5. The measured moisture concentration profiles during drying for (a) fired-clay brick, (b) gypsum and (c) sand–lime brick. The time between subsequent profiles is 5 h for fired-clay brick and gypsum, whereas the time between profiles is 20 h for sand–lime brick. Starting after 10 h the profiles are given for 30 h for fired-clay brick and gypsum, whereas starting after 40 h the profiles are given for 100 h for sand–lime brick. The solid lines give the moisture profiles as determined from directly fitting the analytic model to the measured moisture profiles. The dashed lines indicate the residual moisture θ_∞, observed at 45% relative humidity as used in these drying experiments.

those predicted by the analytic model. The experimental profiles were measured using nuclear magnetic resonance. One-dimensional drying experiments were performed on various samples, i.e. fired-clay brick, gypsum and sand–lime brick. In these experiments the samples were dried using air with a relative humidity of 45%.

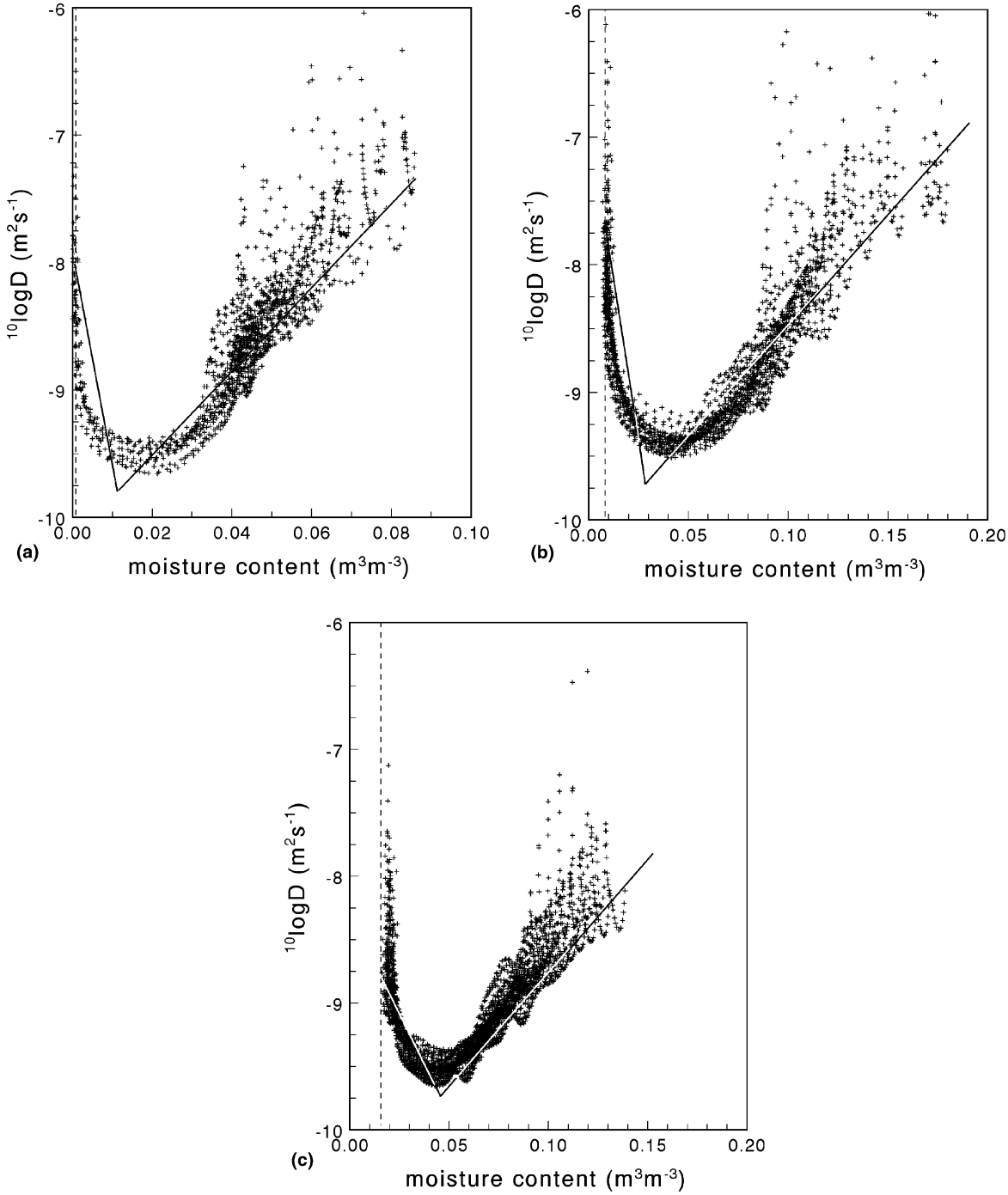

Fig. 6. The moisture diffusivity of (a) fired-clay brick, (b) gypsum and (c) sand–lime brick as determined from measured moisture profiles [4,5]. The solid lines give the moisture diffusivity as determined from directly fitting the analytic model to the measured moisture profiles (see Fig. 5). The vertical dashed lines indicate the residual moisture θ_∞, observed at 45% relative humidity as used in these drying experiments.

An extensive description of these experiments can be found in [5,6].

In Fig. 5 the measured moisture profiles are displayed for various times after the drying front has entered the material for fired-clay brick, gypsum and sand–lime brick. The variations in the measured moisture profiles reflect inhomogeneities in the samples. The analytic model has been fitted to these measured moisture profiles by minimizing the sum of squares (SSQ) defined as

$$\mathrm{SSQ} = \sum_{i=1}^{n} [\theta_{\mathrm{model}}(x,t) - \theta_{\mathrm{measured}}(x,t)]^2, \tag{19}$$

where n is the number of data points (of the order of 135 per profile). This technique will determine the best fit values for $D(\theta_{\mathrm{m}})$, θ_{m}, b_1 and b_2.

The minimum was determined numerically by using standard procedures from the NAG-library. The profiles determined by the fitted analytic model are also plotted in Fig. 5. As can be seen the analytic model describes the moisture profiles especially well for the liquid part of the moisture profile. The drying front is also reproduced very nicely. For all materials the analytic model overestimates the moisture content in the vapour range.

The moisture diffusivity $D(\theta)$ can be determined directly from the experimental moisture profiles by integrating Eq. (1) with respect to x, yielding (see e.g., [5,6])

$$D(\theta) = \frac{\int_L^{x'} (\partial\theta/\partial t)\,\mathrm{d}x}{(\partial\theta/\partial x)_{x'}}. \tag{20}$$

In this equation, use is made of the fact that the partial derivative of θ with respect to x is zero at the vapour right-hand tight bottom ($x = L$). The resulting numerically calculated moisture diffusivities are plotted against the corresponding moisture content in Fig. 6. It is obvious that the data in the figure have a significant scatter, which is rather pronounced at both high and low moisture contents. This is directly related to the accuracy by which the derivative of the moisture content with respect to position can be determined. Despite these uncertainties, however, the data clearly reveal a well-defined variation of the moisture diffusivity with moisture content. An extensive description, including an error analysis, of the procedure for determining the moisture diffusivity is given by Pel et al. [5,6].

Also shown in Fig. 6 are the moisture diffusivities of the analytic model as determined by fitting this model directly to the measured moisture profiles. As can be seen for all materials the moisture diffusivities of the analytic model are within the range of experimentally determined moisture diffusivities.

5. Conclusions and discussion

An analytic solution has been given for the non-linear drying problem. It is shown that the minimum in the moisture diffusivity is related to the drying front. This drying front enters the material with a constant speed determined by the type of material, consistent with experimental results. The speed of the drying front is not only determined by the vapour transport but is also determined by the liquid moisture transport.

The analytic model has been shown to give an accurate solution when compared to the numerical solutions to the non-linear diffusion problem. In comparison with experimental data the analytic model reproduces the liquid part well for both the moisture profiles and the moisture diffusivity. However, the analytic model overestimates the moisture content in the vapour content range. This indicates that in the analytic model the vapour transport is oversimplified by just taking an exponential relation.

The analytic model can be fitted directly to the measured moisture profiles. This is to be preferred over an indirect procedure such as determining the moisture diffusivity from moisture profiles by integrating the time derivative and dividing by the local derivative, which in general results in large experimental error. On this basis the analytic model gives a simple but adequate description of the moisture profiles produced as drying proceeds within a porous material.

Acknowledgements

Part of this project was supported by the Dutch Technology Foundation (STW).

Appendix A

The function α can be approximated by

$$\alpha\left(b_1 U, \frac{b_1}{b_2}\right) = \left(\frac{3}{4b_1 U}\right) \frac{1}{N_{\mathrm{c}}(3/4b_1 U)}. \tag{A.1}$$

Here, in contrast to the original paper [14], g_{r} was taken to be $3/(4b_1 U)$ instead of $1/(2b_1 U)$ when calculating the average slope of $\mathrm{d}g/\mathrm{d}\tau$ as this will give a better match between the numerical calculated and the analytic speed of the drying front.

The function N_{c} is given by

$$\begin{aligned} N_{\mathrm{c}}(g) &= \frac{1}{2}\left[g - K_1 g^2 \ln\left(K_1 + \frac{1}{g}\right) + \frac{1}{K_1}\ln(1 + K_1 g) + K_2 g^2\right] \\ &\quad - \frac{1}{2K_1^3}\left[\ln(1 + K_1 g) - \frac{K_1 g}{1 + K_1 g} - \frac{K_1^2 (1 - K_1)^2 g^2}{2}\right] \end{aligned} \tag{A.2}$$

with the parameters

$$d = \frac{b_1}{b_2}, \tag{A.3}$$

$$K_1 = 1 - b_1 U \tag{A.4}$$

and

$$K_2 = d^2\left(1 + \frac{b_1 U}{d}\right)\ln\left(1 + \frac{b_1 U}{d}\right) - b_1 U(1 + d). \tag{A.5}$$

References

[1] J.R. Philip, D.A. de Vries, Moisture movement in porous materials under temperature gradients, Trans. Am. Geophys. Un. 38 (1957) 222–232.

[2] S. Whitaker, Simultaneous heat, mass and momentum transfer in porous media. A theory of drying porous media, Adv. Heat Transfer 13 (1977) 119–200.

[3] J. Bear, Y. Bachmat, Introduction to Modelling of Transport Phenomena in Porous Media, vol. 4, Kluwer, Dordrecht, 1990.

[4] L. Pel, A.A.J. Ketelaars, O.C.G. Adan, A.A. van Well, Determination of moisture diffusivity in porous media using scanning neutron radiography, Int. J. Heat Mass Transfer 36 (1993) 1261–1267.

[5] L. Pel, H. Brocken, K. Kopinga, Determination of moisture diffusivity in porous media using moisture concentration profiles, Int. J. Heat Mass Transfer 39 (1996) 1273–1280.

[6] L. Pel, Moisture transport in porous building materials, Ph.D. Thesis, Eindhoven University of Technology, The Netherlands, 1995.

[7] O. Krischer, Die wissenschaftlichen Grundlagen der Trocknungstechnik, Springer, Berlin, 1978.

[8] H. Garrecht, Porenstrukturmodelle für den Feuchtehaushalt von Buastoffen mit und ohne Saltzbefrachtung und rechnerische Anwendung auf Mauerwerk, Ph.D. Thesis, University of Karlsruhe, Germany, 1992.

[9] A.A.J. Ketelaars, Drying deformable media, Ph.D. Thesis, Eindhoven University of Technology, The Netherlands, 1992.

[10] B. Kroes, The influence of the material properties on the drying kinetics, Ph.D. Thesis, Eindhoven University of Technology, The Netherlands, 1999.

[11] O.C.G. Adan, On the fungal defacement of interior finishes, Ph.D. Thesis, Eindhoven University of Technology, The Netherlands, 1994.

[12] J. van der Kooi, Moisture transport in cellular concrete roofs, Ph.D. Thesis, Delft University of Technology, The Netherlands, 1971.

[13] P. Crausse, G. Bacon, S. Bories, Etude fondamentale des transfert couples chaleur-masse en milieux poreux, Int. J. Heat Mass Transfer 24 (1981) 991–1004.

[14] J.R. Philip, Theory of infiltration, Adv. Hydrosci. 5 (1969) 215–305.

[15] K. Kießl, Kapillarer und dampfförmiger Feuchtetransport in mehrschichtigen Bauteilen. Rechnerische Erfassung und bauphysikalische Anwendung, Ph.D. Thesis, University of Essen, Germany, 1983.

[16] H. Künzel, Simultaneous heat and moisture transport in building components one- and twodimensional calculation using simple parameters, Ph.D. Thesis, University of Stuttgart, Germany, 1995.

[17] M. Krus, Feuchtetransport und Speicherkoeffizienten poröser mineralischer Baustoffe Theoretische Grundlagen und neue Meß techniken, Ph.D. Thesis, University of Stuttgart, Germany, 1995.

[18] K.A. Landman, L. Pel, E.F. Kaasschieter, Analytic modelling of drying of porous materials, Math. Eng. Ind. 8 (2001) 89–122.

[19] J. van Brakel, Mass transfer in convective drying, Adv. Drying 1 (1980) 217–267.